

## Contribution of molecular flexibility to the elastic–plastic properties of molecular crystal -RDX

This content has been downloaded from IOPscience. Please scroll down to see the full text.

2017 Modelling Simul. Mater. Sci. Eng. 25 015006

(<http://iopscience.iop.org/0965-0393/25/1/015006>)

View [the table of contents for this issue](#), or go to the [journal homepage](#) for more

Download details:

IP Address: 128.113.213.184

This content was downloaded on 07/12/2016 at 16:38

Please note that [terms and conditions apply](#).

# Contribution of molecular flexibility to the elastic–plastic properties of molecular crystal $\alpha$ -RDX

Anirban Pal and Catalin R Picu

Department of Mechanical, Aerospace and Nuclear Engineering, Rensselaer Polytechnic Institute, Troy, NY 12180, USA

E-mail: [picuc@rpi.edu](mailto:picuc@rpi.edu)

Received 20 June 2016, revised 4 November 2016

Accepted for publication 11 November 2016


Published 7 December 2016



CrossMark

## Abstract

We show in this work that the mechanical properties of molecular crystals are strongly affected by the flexibility of the constituent molecules. To this end, we explore several kinematically restrained models of the molecular crystal cyclotrimethylene trinitramine in the  $\alpha$  phase. We evaluate the effect of gradually removing the flexibility of the molecule on various crystal-scale parameters such as the elastic constants, the lattice parameters, the thermal expansion coefficients, the stacking fault energy and the critical stress for the motion of a dislocation (the Peierls–Nabarro stress). The values of these parameters evaluated with the fully refined, fully flexible atomistic model of the crystal are taken as reference. It is observed that the elastic constants, the lattice parameters and their dependence on pressure, and the thermal expansion coefficient can be accurately predicted with models that consider the  $\text{NO}_2$  and  $\text{CH}_2$  groups rigid, and the N–N bonds and the bonds of the triazine ring inextensible. Eliminating the dihedral flexibility of the ring leads to larger errors. The model in which the entire molecule is considered rigid or is mapped to a blob leads to even larger errors. Only the fully flexible, reference model provides accurate values for the stacking fault energy and the Peierls–Nabarro critical stress. Removing any component of the molecular flexibility leads to large errors in these parameters. These results also provide guidance for the development of coarse grained models of molecular crystals.

 Online supplementary data available from [stacks.iop.org/MSMS/25/015006/mmedia](http://stacks.iop.org/MSMS/25/015006/mmedia)

Keywords: molecular crystals, coarse graining, dislocations

(Some figures may appear in colour only in the online journal)

## 1. Introduction

While most engineering crystalline materials, such as metals, ceramics and semiconductors are monatomic, a large and diverse class of crystals exist in which the repeat unit is an entire molecule. Examples of molecular crystals are ice, sugar, most pharmaceuticals and energetic materials.

The importance of the mechanical behavior of pharmaceutical molecular crystals is related to powder processability and to the stability of the desired phases of the active substance. It is known that certain phases of given substance have better bio-availability than others [1] and some phases are toxic [2].

Energetic materials are substances that release large amounts of energy at very high rates when decomposing. They are mixed with polymers to form composites used as explosives (polymer-bonded explosives, PBX) or with oxidizers to produce solid propellants. Their performance is related to the energy released per unit mass and per unit time. The mechanical behavior of these materials is of importance since the chemical reaction leading to detonation may be initiated by deformation. Furthermore, the need to reduce the sensitivity of the material to unintentional detonation requires gaining control on the fundamental processes that link mechanics with chemical decomposition.

In this work we investigate the role of molecular flexibility in the mechanics of molecular crystals, with focus on one of the most common energetic materials, cyclotrimethylene trinitramine (RDX). Molecules take certain conformational states in the crystal. For example, the RDX molecules in vacuum sample a broad range of configurations, with the nitro groups ( $\text{NO}_2$ ) wagging about the central triazine ring. The ring itself may flip between the chair and boat configurations. In the crystal, the molecule is in the C<sub>3h</sub> conformational state, i.e. two of the nitro groups are oriented in the axial direction of the ring, while the third is oriented equatorially [3]. The ring is in the chair configuration. Conformational changes are difficult in the condensed phase due to packing, but not impossible. It has been shown that conformational changes can take place in the core of dislocations, at stacking faults [4, 5] and at free surfaces, including those of voids [6]. Hence, evidence exists that lower energy states can be reached if the molecules are allowed to relax. However, to what extent this intra-molecular relaxation contributes to defining the key parameters of the mechanics of the crystal is not entirely clear. The present work aims to clarify this issue for the case of the  $\alpha$  phase of RDX, which is the stable phase of RDX in ambient conditions.

The study of the role of molecular flexibility in mechanics is also important for developing coarse grained (CG) models of these materials. Coarse-graining is a process by which an existing model is reconfigured to operate on larger spatiotemporal scales by a reduction of the set of degrees of freedom (DOFs) of the system. This usually entails loss of information and a decrease of the system entropy. Whether this information loss is acceptable depends on the scale and type of physical phenomena that the CG model aims to reproduce. Coarse graining can be applied at the sub-molecular level, where a group of atoms within a molecule is represented as a bead (united atom), or at the supra-molecular level, where one or multiple molecules are represented by a supra-molecular 'bead'. This is typically done for polymers [7] and bio-macromolecules [8].

Although the above-mentioned methods have proved to be suitable for systems lacking long-range order, such as polymeric melts, the extension of these ideas to molecular crystals is not straightforward. The symmetry of the crystal poses limitations on the shape and nature of the CG particles and potentials, as they may not be able to accurately reproduce the space group and hence the packing of the condensed phase. Furthermore, a clear separation of frequencies between the coarsened DOF and atomic DOF may not exist. This is especially

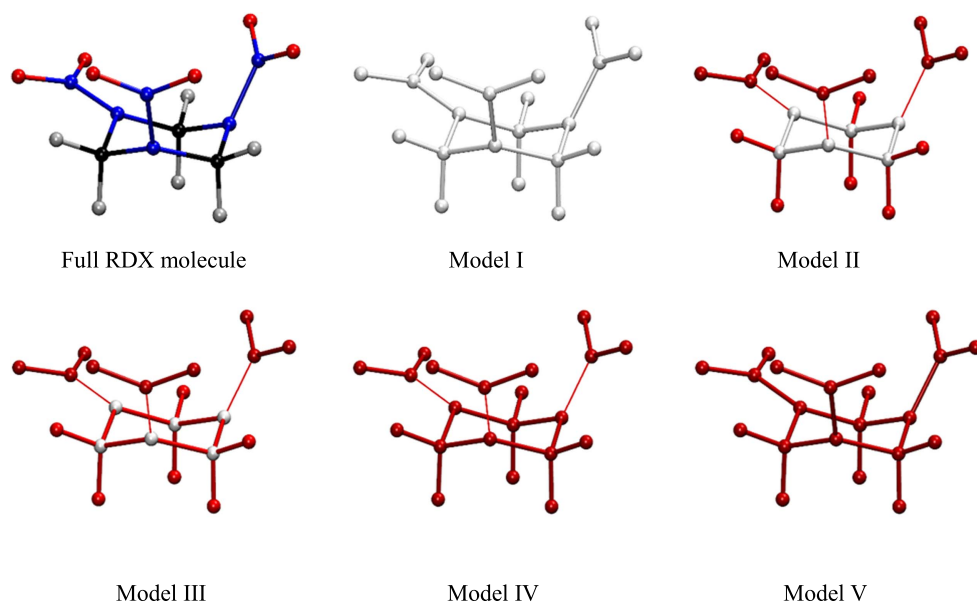


**Figure 1.** Schematic representation of the models used in this study. The full RDX molecule is shown in the upper left panel, with C atoms shown in black, N in blue, O in red and H silver. Model I is fully flexible (in the following panels gray indicates ‘flexible’) while Model V is a fully rigid body (in the following panels red indicates ‘rigid’). In Model II, the triazine ring is flexible, while the NO<sub>2</sub> and CH<sub>2</sub> groups are rigid bodies and N–N bonds are inextensible (thin red lines). The nitro groups are free to rotate about the N–N bond. Model III preserves all features of Model II and, in addition, the length of the bonds of the ring is constrained. The ring is deforming via dihedral/angle motions in this model. Model IV is similar to Model III except that now the triazine ring and the CH<sub>2</sub> groups belong to a single rigid body. Model V is fully rigid.

true for energetic molecular crystals as the lattice modes are coupled to the wagging of the nitro-groups (intra-molecular vibrations) [9] and the distortion of the heterocyclic ring, and hence taking the most obvious coarsening step, i.e. representing a molecule by a bead or a set of beads may not be ideal. Also, the properties that are often of interest in the crystalline phase, such as formation and migration of defects (vacancies, dislocations, twins, grain boundaries) are very different in nature from those in melts (glass transition, diffusion) and rely heavily on the accurate representation of the crystalline environment. Even if such model were designed to represent accurately a particular molecular crystal in the context of the properties discussed above, it is not clear whether it would be transferable to another molecular crystal of similar chemical composition.

In order to tackle these challenges, the field of CG modeling in energetic molecular crystals has garnered recent attention. A CG model was developed for PETN [10] via experimental fitting, which reproduces well lattice constants, sublimation energy, and pressure-volume curves. A dissipative particle dynamics (DPD) CG model was developed for TATB [11] to model the kinetics of energy transfer between intramolecular (vibrons) and extra-molecular (lattice phonons) DOFs. Recent studies on nitromethane [12] and RDX [13, 14] have investigated the applicability of the force matching-based multiscale coarse-graining (MS-CG) method [15, 16]. In [12], a density dependent MS-CG potential was

developed for nitromethane which accurately reproduced shock Hugoniot curves. The MS-CG potential for RDX reproduces crystal structure, elastic constants, melting point, and pressure–volume isotherms [13] and was recently modified to improve energy conservation [14].

In this work we construct a series of RDX crystal models in which the molecules have decreasing degrees of flexibility and we investigate the effect of such constraints on (i) the elasticity of the crystal, (ii) the crystal symmetry and lattice constants, (iii) thermal expansion, and (iv) the stacking fault energy and critical stress for dislocation motion (the Peierls–Nabarro (PN) stress). We deem these parameters central to the proper representation of the elastic-plastic behavior of a crystal. The inter-atomic interactions are described by the force field relevant for the fully refined atomistic model. The study indicates which components of the molecular flexibility are of importance with respect to each of the parameters listed above. It also provides guidance for developing CG representations of the crystal by indicating the acceptable coarse graining level if certain level of performance is desired.

## 2. Methods

The RDX molecule has 21 atoms and hence 63 DOFs. If the flexibility of the molecule is entirely restricted, the resulting rigid object has 6 DOFs which are required in order to preserve the crystal space group. To study the effect of molecular flexibility on the mechanical properties of the crystal, we develop a set of five models (figure 1). Model I represents the fully refined, fully flexible molecule in which all 63 DOFs are present as independent variables. This model is used in regular models of RDX [17, 18] and represents the reference for the present study. In Model II, the NO<sub>2</sub> and CH<sub>2</sub> groups are made internally rigid (C–H, N–O bonds and H–C–H, O–N–O angles frozen) and the N–N bonds are rendered inextensible, but the wagging motion of the NO<sub>2</sub> groups relative to the ring as well as the rotation of the nitro group about the N–N bond are allowed. In Model III we preserve all features of Model II and also render the bonds of the triazine ring essentially inextensible, while preserving the angular/dihedral flexibility of the ring. The nitro groups are still free to wag relative to the ring in this representation. Model IV preserves all these features and, in addition, the angular/dihedral motion of the ring is restricted. In this model, the molecule is composed from a rigid ring and three rigid nitro groups that are free to move relative to the ring. Model V is that of a fully rigid RDX molecule. In all cases, the groups of atoms constrained to be rigid are held in the configuration they have in the perfect crystal at 0 K. The structure of the various models is summarized in figure 1.

This procedure differs from a regular CG method in two regards. The parts of the molecule whose structure is not allowed to change during motion are not replaced by ‘blobs’, i.e. spherical or ellipsoidal entities. Furthermore, since all atoms of the fully refined model are present in all models of figure 1 (although parts of the molecule are rendered rigid), the interactions are evaluated with the full force field used for the reference model (Model I).

The force field used for all models is the Smith–Bharadwaj (SB) potential [19], which was developed using quantum chemistry calculations to reproduce structural properties for cyclotetramethylene tetranitramine (HMX) and dimethyl dinitro methyldiamine (DDMD). This potential can reproduce elastic and thermal properties of RDX [17, 20], and has been used to study crystal nanomechanics [18], high pressure states [17], melting [21], vibrational properties [9], absorption spectra [22], phase transformations during shock [23], dislocations [4, 24–27], and rotational defects [5].

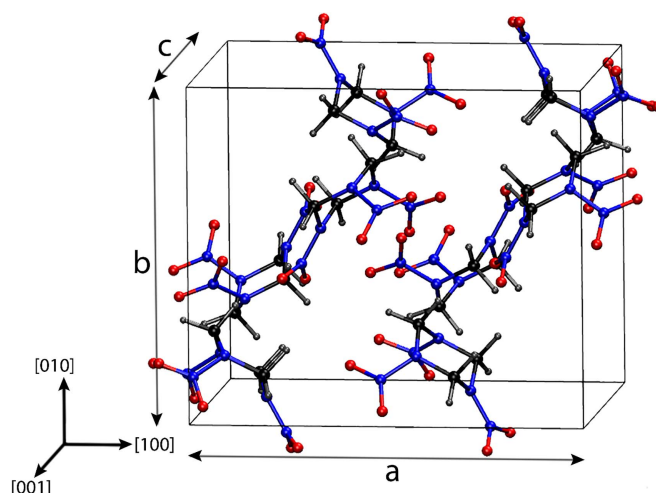


**Figure 2.** Unit cell of  $\alpha$ -RDX with lattice parameters  $a = 13.37 \text{ \AA}$ ,  $b = 11.33 \text{ \AA}$ , and  $c = 10.35 \text{ \AA}$  after relaxation to 1 atm, 0 K using the SB potential.

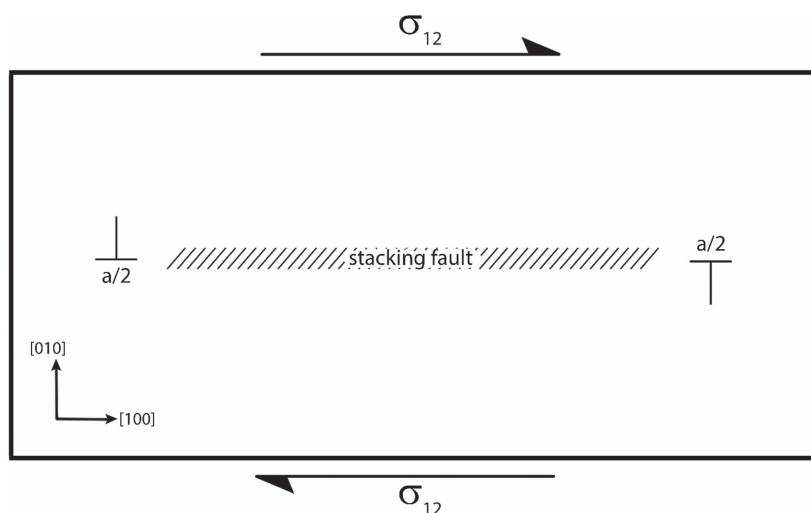


**Figure 3.** Schematic of the setup used for computing PN stress including a dipole of positive and negative  $1/2 [100](010)$  partials separated by a stacking fault. The far field is applied as shown in the figure, pushing the two partials toward each other.

Each of these five models was subjected to various tests to determine which model provides the best balance between accuracy and computational efficiency. The models are compared in terms of their prediction of lattice constants, elastic constants of the perfect crystal, coefficient of thermal expansion, the PN stress and stacking fault energies. For the elastic, pressure–volume ( $P$ – $V$ ) and thermal expansion calculations, a  $5 \times 5 \times 5$  ( $66.4 \text{ \AA} \times 56.7 \text{ \AA} \times 51.8 \text{ \AA}$ ) periodic supercell aligned with the orthogonal principal crystallographic axes  $x_1 \equiv [100]$ ,  $x_2 \equiv [010]$ ,  $x_3 \equiv [001]$  was used. In these models the molecules were arranged as in the perfect crystal structure obtained from neutron diffraction data

[28] (figure 2) and relaxed with the SB potential using the fully flexible model. To calculate the orthotropic elastic moduli, the supercell was deformed affinely in three orthogonal and three shear modes by 0.5% strain and relaxed to 0 K, using NVT integration and viscous damping. To compute  $P$ - $V$  curves, the molecular dynamics of the supercell was integrated at finite temperatures using a constant pressure (NPT) barostat [29], and the volume at 0 K was estimated after slow cooling via viscous damping. The coefficient of thermal expansion was estimated similarly by measuring the mean supercell dimensions at 1 atm pressure and various target temperatures, within the NPT ensemble. For the above cases, dynamics of the rigid bodies was integrated using special thermostats which regulate both their translational and rotational DOFs [30], and the inextensible N-N bonds were implemented via SHAKE [31] constraints. Further details on these models and simulation procedures are presented in the supplementary material.

A larger system of  $50 \times 25 \times 2$  ( $671.4 \text{ \AA} \times 434.0 \text{ \AA} \times 21.4 \text{ \AA}$ , in the [100], [010], [001] directions respectively) unit cells containing a partial edge dislocation dipole (figure 3), each of the partials of the dipole having Burgers vector  $b = 1/2[100](010)$ , was used for the PN stress calculations. The dipole was inserted by translating the centers of mass (COM) of the molecules by the Volterra displacement field. These models were periodic in the direction of the dislocation line (direction [001]) and in the [100] direction. A free surface boundary condition (vacuum padding) was applied on the boundaries parallel to the glide plane, (010). This slip system has been reported to have the lowest PN stress and hence is expected to be the most active in RDX [24]. The full Burgers vector edge dislocation in this crystal direction is not stable [24] and dissociates in two pure edge partials of equal Burgers vector,  $1/2[100](010)$ . Considering a dipole (as opposed to a single partial) reduces the image effects and allows containing the stacking fault separating the two partials within the simulation cell. The distance between partials is selected such that the dipole is in equilibrium in the unloaded configuration. Note that the attractive interaction of the two partials and the effect of the stacking fault are balanced by the interaction with images across the periodic boundaries.

This model was used instead of the more usual dipole of full dislocations due to the observations made in MD simulations of RDX crystals subjected to shock [4] that individual partials move across entire grains leaving long stacking fault trails behind. This deformation mode is similar to that observed in molecular simulations of nanocrystalline materials [32], although the physics in the two cases is somewhat different. Therefore, the PN stress of a partial is of importance for the plastic deformation of these crystals.

In models containing dislocation cores, using rigid interactions for models II-V created dynamic stability problems. Therefore, we replaced the rigid interactions with interactions 50 times stiffer than in Model I. This reduces the deformation of the respective bonds and angles by an order of magnitude relative to the fully refined model and hence the intended rigid behavior is reasonably reproduced. The penalty for this approximation is integration with a smaller time step. Constant shear stress simulations ( $\sigma_{12}$ ) were performed using this setup at 0.01 K, with the simulation cell volume kept fixed. The free surfaces (vacuum padding) ensured that there was no normal stress on the glide plane. The far field was gradually increased and the critical stress at which stability was lost during relaxation was recorded and used to compute the PN stress. The other interactions balance each other in the unloaded configuration and should not be considered in this estimate. This method is similar to that used in previous work [24].

Stacking fault energies (SFE) were obtained using a fully periodic  $3 \times 24 \times 3$  ( $40.1 \text{ \AA} \times 272.0 \text{ \AA} \times 31.05 \text{ \AA}$ ) supercell. To create the stacking fault, the upper half of the supercell containing  $3 \times 12 \times 3$  cells was displaced by the stacking fault vector of  $1/2 [100](010)$  relative to the lower part, resulting in the creation of two stacking fault surfaces (one in

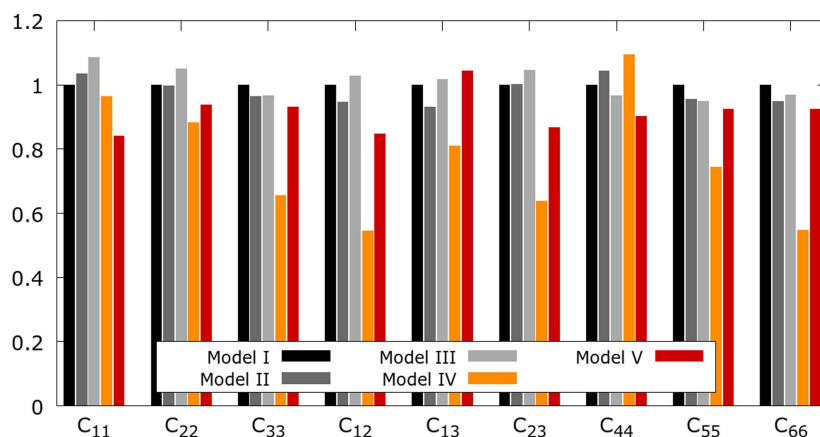


**Figure 4.** Elastic moduli (Voigt notation) at 0 K computed in the coordinate system aligned with the principal crystallographic directions and predicted using Models I–V (vertical bars). Values are normalized with the prediction of the fully flexible Model I. In each stack the columns from left to right correspond to Models I–V.

the middle and one at the top/bottom periodic boundary). This system was relaxed using isobaric-isothermal (NPT) integrators at 1 atm and finite temperatures, followed by slow cooling (viscous damping), after which the energies were recorded. Vibrational DOS were computed using the velocity autocorrelation function, whose Fourier Transform was used to compute the density of states [33]. All simulations were performed using LAMMPS [34]. Further information regarding the set-ups used to perform these simulations is provided in the Supplementary material.

### 3. Results and discussion

In this section we compare the five models presented in figure 1 based on their ability to predict various material and structural parameters.

#### 3.1. Elastic, structural and thermal properties

Figure 4 shows the variation of the 0 K elastic moduli (Voigt notation) evaluated in the principal crystal directions for each model. The values are normalized by the elastic constants predicted by the fully refined Model I, which are reported in table 1. The coefficients of thermal expansion in the principal directions evaluated with Model I are also reported in table 1. Similar results have been reported in literature based on experimental [35–40] and computational [17, 41, 42] studies. Table 1 include values computed using dispersion-corrected density functional theory (DTF-D3) and reported in [42] and experimental values obtained from measurements performed at 300 K by Brillouin spectroscopy [35]. Good agreement of these experimental values with data obtained from other experiments [37, 38, 40] is reported. The results of this work should be compared with the DFT calculations since both correspond to 0 K. The table also presents thermal expansion coefficients computed with the fully refined model. These are compared with similar values obtained computationally [17] and corresponding to the temperature range 250–350 K. Experimental values are also presented [36, 39].



**Table 1.** Orthotropic elastic constants obtained using the fully flexible model (Model I) at 0 K. Also shown are the coefficients of thermal expansion (CTE) obtained using Model I, averaged over the temperature range 250–350 K. These constants are used to normalize the data in figures 4 and 6. Computational and experimental results from literature are shown for comparison.

	Elastic constants (GPa)			Coefficients of thermal expansion ( $10^{-5} \text{ K}^{-1}$ )			
	This work (0 K)	DFT (0 K) [42]	Expt. (300 K) [35]		This work	Atomistic [17]	Expt. [36]
C11	29.5	25.7	25.8	$\alpha$ [100]	3.34	3.03	2.70
C22	28.1	20.8	20.1	$\alpha$ [010]	6.32	6.16	8.70
C33	29.6	21.9	18.9	$\alpha$ [001]	6.36	7.19	8.00
C12	14.0	7.74	8.3				
C13	8.6	4.42	6.4				
C23	10.9	7.02	6.4				
C44	3.8	5.86	5.3				
C55	6.5	4.62	4.2				
C66	10.3	7.29	7.2				

The elastic constants predicted by Models II and III agree to within 10% with those predicted using Model I (figure 4). Model V predictions are within 16% of those of Model I, and Model IV shows significant deviations. The agreement of  $C_{11}$ ,  $C_{22}$ , and  $C_{33}$  is of importance because these constants determine the longitudinal wave speed in the crystal. We conclude that Models II and III are adequate for representing the dynamics of the perfect crystal. The agreement indicates that coarse graining the nitro and methylene groups does not noticeably affect the longitudinal wave speed. The fact that Model IV does not agree with Models I–III indicates that ring flexibility is important for wave propagation. This was also demonstrated in the context of the crystal vibrational behavior [9] where the rigid molecule approximation could account for only 48 of the 72 observed lattice phonon bands, and the remaining phonon bands had some degree of coupling to intra-molecular modes of deformation, specifically the N–N bonds. For the shear moduli the picture is similar except for Model IV which differs significantly from the Model I predictions. This has implications for the long-range field of screw dislocations oriented parallel to the principal crystal axes.  $C_{12}$ ,  $C_{13}$ , and  $C_{23}$  predicted with Models I–III agree well, but the departure is significant for models IV and V, which perform the poorest.

Further, we study the variation of the lattice constants with pressure. We limit the analysis to pressures below 3.5 GPa, which is smaller than the experimental  $\alpha$ – $\gamma$  phase transition pressure of 3.9 GPa [43]. (Although the  $\alpha$ – $\gamma$  phase-transition, using the SB potential, has not been computationally reproduced up to 10 GPa, the  $\gamma$ – $\alpha$  transition has been shown to occur at 2.1 GPa [17]). This variation is shown in figure 5. All models, except Model V, exhibit a similar trend and although lattice constants are different, deviations are smaller than 3%. The bulk moduli computed based on the data in figure 4 are in agreement with the variation of the lattice constants with pressure at small elastic perturbations.

There is some disagreement in literature about the compressibility behavior of  $\alpha$ -RDX [41, 42]. Some studies [38, 41, 44] report nearly isotropic compressibility in the (001) plane (directions [100] and [010]), while others [37, 40] indicate higher compressibility in the [010] direction compared to the [100] direction. However, all reports agree that the [001] direction

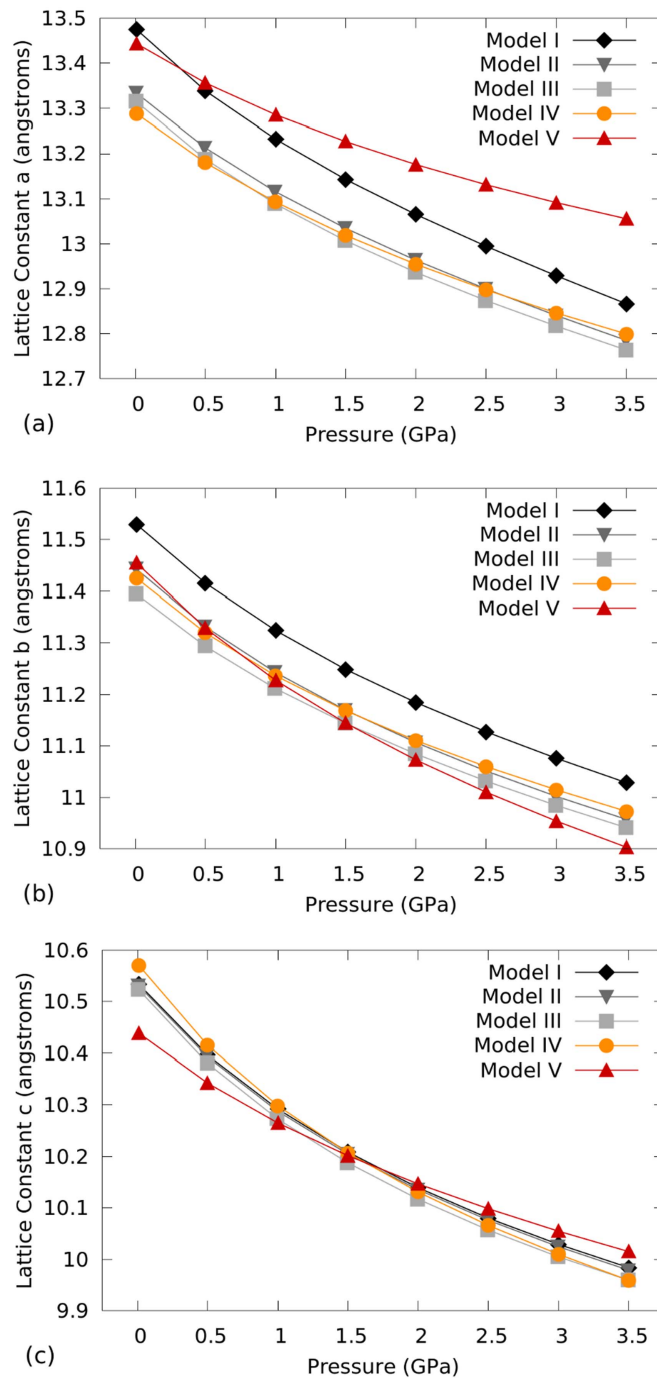


**Figure 5.** Variation of lattice constants with pressure as predicted by the various models at 0 K. The three panels correspond to the three lattice constants, (a)–(c) measured in principal crystallographic directions (figure 1).

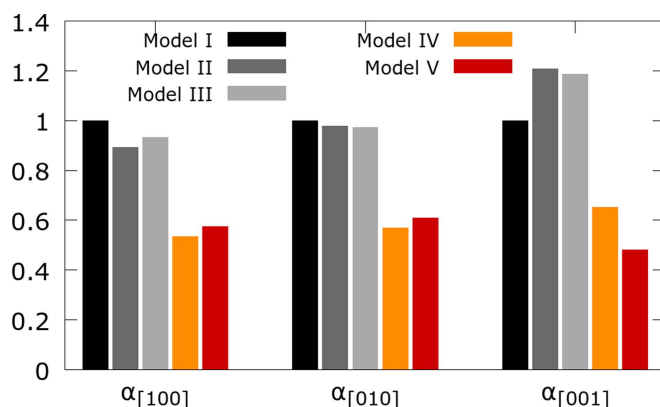


**Figure 6.** Normalized coefficients of thermal expansion in the three principal directions of the crystal and at zero pressure. The values reported here are averages over the temperature range 250–350 K and are normalized with the respective coefficients predicted using Model I (shown in table 1). In each stack, the columns from left to right correspond to Models I–V.

is the most compressible. Our calculations indicate that for Models I–IV, the compressibility in directions [100] and [010] is almost identical, while the [001] direction is the most compressible. For Model V, the behavior changes, with the [010] direction becoming most compressible, followed by [001] and then [100] directions.

Thermal expansion stems from the anharmonicity of the crystal potential [45]. Since the total crystal potential used here is not harmonic, although comprising interaction terms may be harmonic (such as bonds, angles, dihedrals), the system is expected to exhibit a finite thermal expansion coefficient. In the quasi-harmonic approximation (QHA), the thermal expansion coefficient is related to the variation of vibrational frequencies with volume, through the Grüneisen parameters [46], which depend non-trivially on the individual interaction terms present in the crystal Hamiltonian. Figure 6 shows the coefficient of thermal expansion (CTE) computed in the principal crystallographic directions for the various models and averaged over the temperature range 250–350 K. The coefficients remain approximately constant in this temperature range (vary by less than 9%) for given model realization. The values are normalized by the prediction of Model I (table 1). As before, the agreement of models I to III is favorable and the disparity of models IV and V is again encountered. Thermal expansion in molecular crystals can depend acutely and non-trivially on molecular structure and flexibility, as demonstrated by recent work [47] where large positive and negative anisotropic thermal expansion coefficients in a diyn-diol crystal was attributed to molecular tilting during heating. The dihedral and angular flexibility of the triazine ring is reduced in models III, IV and V suggesting that ring flexibility contributes significantly to the CTE.

### 3.2. Crystal defects

The properties discussed so far reflect the perfect crystalline lattice environment, devoid of defects. The effect of molecular flexibility on the structure, stability and motion of dislocations is important for understanding the plastic deformation of such crystals. This was investigated in detail previously with the fully refined model (Model I) [24]. In this reference, dislocations residing on various glide systems were considered and their stability and PN

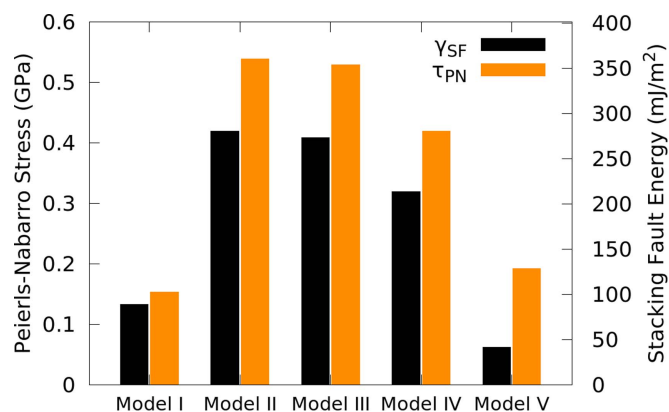


**Figure 7.** Peierls stress (orange) for a partial edge dislocation of Burgers vector  $1/2$  (010)[100] and the associated stacking fault energy (black) computed with Models I–V.

stresses were computed. Here we consider only the dislocation with the lowest PN stress—the partial pure edge dislocation of Burgers vector  $1/2$  [100](010)—which is considered in the literature to contribute significantly to plasticity in this material. Plastic activity in the (010) plane has been observed experimentally [48–51] and in computer simulations [4]. We use the five models of figure 1 to represent this type of dislocation.

The simulation setup used in this part of the investigation is described in section 2. It contains two partials of same Burgers vector and opposite sign, separated by a stacking fault (figure 3). We compute the PN stress (shear stress resolved in the direction of the Burgers vector) required to put the partials in motion. It is also relevant to see how the stacking fault energy is affected by restricting molecular flexibility. Figure 7 shows the values of these two quantities predicted with the various models.

The PN stress ( $\tau_{PN}$ ) is observed to be very sensitive to molecular flexibility. The applied stress at which either partial starts moving predicted with Models II–IV increases drastically relative to the reference Model I. The stacking fault energy increases 3 times upon coarse graining (models II–IV).  $\tau_{PN}$  drops for Model V but stays above the reference, while the stacking fault energy drops below the value predicted with the fully flexible Model I.

The steep rise of the PN stress and the stacking fault energy appear to be associated with the limited flexibility of the molecules. Preventing molecular distortion limits the ability of the system to reach low energy states in the process of overcoming the Peierls barrier. The stacking fault energy is computed as the difference between the energy of the crystal with a  $1/2$  [100](010) stacking fault,  $E_{SF}$ , and the energy of the corresponding perfect crystal,  $E_0$ . The PN stress for the partial is computed as the critical applied stress minus the stress resulting from the action of the stacking fault on the dislocation. The decrease of the PN stress in the case of Model V is due to a lower stacking fault energy. The lower  $\gamma_{SF}$  in this case is due to the poor packing of the rigid molecules in the perfect crystal, which results in a larger  $E_0$ . At the same time,  $E_{SF}$  is not substantially affected and hence the difference  $\gamma_{SF} = E_{SF} - E_0$  decreases relative to Model I. For Models II–IV, both the PN stress and  $\gamma_{SF}$  are larger than the values corresponding to Model I. The change of PN stress from one model to the other is not associated with core distortions in the unloaded state. The unloaded core profiles evaluated with the five models overlap to a very good approximation.

The large discrepancy in the prediction of basic dislocation-related quantities demonstrated by the data in figure 7 brings into doubt the usefulness of any level of this type of

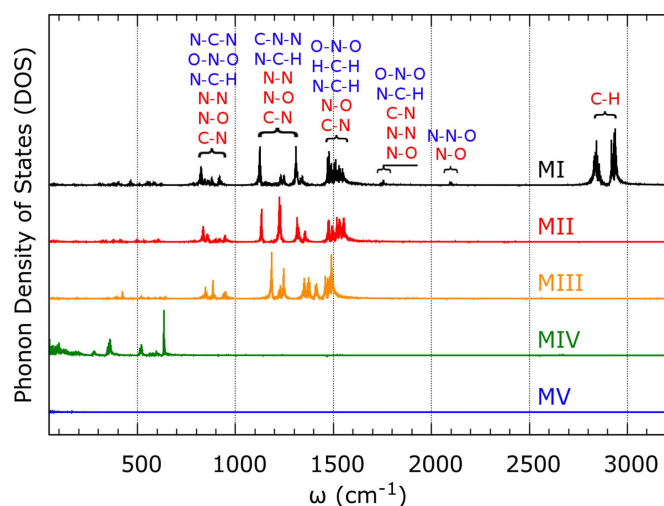


**Figure 8.** Phonon density of states for Models I–V, indicating the effect of limiting molecular flexibility on the phonon spectrum. The peaks are associated with specific bonds and angles, as indicated in red and blue, respectively [9]. The peaks near 2940, 2865, 2110 and 1760  $\text{cm}^{-1}$  disappear for Models II and III (denoted by MII and MIII). For Model IV (MIV), the highest frequency is at 635  $\text{cm}^{-1}$ . For the completely rigid Model V (MV), the spectrum is flat above 100  $\text{cm}^{-1}$ . The spectrum is shown from 50 to 3200  $\text{cm}^{-1}$ .

coarse graining in models used to study dislocation activity in RDX. This agrees with the conclusion of a previous study [26], where allowing for molecular flexibility and reorientation was found to be necessary to accurately capture dislocation nucleation and partial core structures in  $\alpha$ -RDX.

The simple models presented above qualitatively indicate the DOFs that should be present in a coarse-grained model for accurate representation of the elastic–plastic behavior. To summarize, the agreement of the elastic moduli with the reference Model I is good for Models II and III and poor for Models IV and V. Pressure–volume curves display similar trends for Models I–IV but Model V stands out. Thermal expansion coefficients are also within acceptable limits for Models II and III. For slip on the most active slip system, i.e.  $\frac{1}{2}$  [100](010), all models display egregious differences.

### 3.3. Vibrational density of states

The above analysis has focused on gradually limiting the primary modes of deformation of the molecule (stretching of N–N bonds, wagging of  $\text{NO}_2$  groups, ring flexibility, etc) and assessing the impact of such constraints on the elastic, thermal and plastic properties of the crystal. It is also of interest to determine how restricting molecular flexibility changes the vibrational density of states (VDOS).

In relation to coarse graining, in order to simulate longer physical times, it is necessary to use larger time-steps during integration, which is typically enabled by coarsening out the intra-molecular features that are associated with the highest frequencies observed in VDOS. We computed the VDOS of the  $\alpha$ -RDX crystal, which is shown in figure 8. This is similar to the VDOS previously reported for the same crystal [9, 52]. The major molecular deformation

modes (bond and angle deformations) that contribute to the peaks in the VDOS plot are indicated in figure 8 (referred from [9]).

Figure 8 shows a comparison of the VDOS computed with Models I–V. Rendering the  $\text{CH}_2$  group rigid eliminates the twin peaks located in the vicinity of  $\omega = 2900 \text{ cm}^{-1}$ ; these correspond to a time period of  $\sim 11.5$  fs. The peak at  $2100 \text{ cm}^{-1}$  is associated with the vibration of N–O bonds and N–N–O angles, so making the  $\text{NO}_2$  groups rigid and freezing the N–N–O bond will dispel this peak. This corresponds to Model II, which, because of the loss of the  $1760 \text{ cm}^{-1}$  peak as well, represents a crystal with highest frequency  $\omega \sim 1600 \text{ cm}^{-1}$ . The corresponding time period is 20.8 fs and hence Model II can be integrated with a time step approximately twice larger than that used for Model I. Note that in this model the wag mode of the  $\text{NO}_2$  groups is preserved, but the associated frequency is that of the N–C–N angle which is in the range  $300\text{--}800 \text{ cm}^{-1}$ .

Restricting further the molecular flexibility renders the C–N bonds of the ring rigid. This reduces the highest frequency peaks to  $\omega \approx 1500 \text{ cm}^{-1}$ , dependent only on N–C–H angle vibrations as all other contributing modes have been removed. If we proceed further and make the entire ring rigid, but with the  $\text{NO}_2$  groups still free to wag (Model IV), the highest frequency becomes  $\omega = 635 \text{ cm}^{-1}$ , which corresponds to a time period of  $\sim 52.5$  fs. Note that the frequency spectrum is truncated at  $50 \text{ cm}^{-1}$  as lower frequencies cannot be sampled accurately within the time window of the simulation procedure (see supplementary material).

In conclusion, corroborating the results of this section with those of sections A and B, as long as one is concerned with perfect crystals, Models II or III should be used, which would allow increasing the time step of the integration from  $\sim 1$  fs (for the fully refined Model I) to 2 fs. Larger time steps can be used for Models IV and V, but the accuracy with which these models predict the elastic constants and the thermal expansion coefficient is lower. In order to properly capture crystal defect mechanics one needs to use the fully refined model (I) which has to be integrated with a time step of 1 fs.

### 3.4. Computational aspects and implications for developing CG models

The central objective of developing coarse-grained models is the minimization of the associated computational costs in order to maximize the range of spatial-temporal scales that can be represented, while still capturing properly the physics of interest. In this context, it may be useful to take a closer look at the computational costs associated with the force-field used in this work.

Let us evaluate the computational expense associated with computing the various interatomic interactions represented in the reference Model I. To this end we use the IBM BlueGene/Q super-computer with 512 processors. For a system of  $5 \times 5 \times 5$  unit cells of  $\alpha$ -RDX with  $N = 21\,000$  atoms and a  $15 \text{ \AA}$  pair-wise cutoff, the average number of neighbors per atom is approximately 1100. Non-bonded pairwise force computations are responsible for about 71% of the computation time while the  $K$ -space long-range solver takes 19% of the time. The bond, angular, and dihedral interactions take less than 1% of the time, and they scale linearly with  $N$ . Since total pairwise computations scale as  $N^*N_n$  ( $N_n =$  number of atoms within neighbor list), lowering the number of variables by a factor of  $r$  can lead to an  $r$ -fold reduction in the number of force computations. For the long-range solver which scales as  $N^*\log(N)$ , a coarser charge grid can produce a super-linear speed-up.

The RDX molecule has 21 atoms. The six hydrogen atoms can be trivially CG by replacing the methylene groups by dipoles owing to their small size and lack of hydrogen-bonding ability. If we look at the candidate models presented so far, the nitro groups may also be replaced by dipoles, as they have a significant net moment. This removes three more

**Table 2.** Charges [53] and moments on the RDX molecule.

Atom	Charge ( $e$ )
Carbon (black)	-0.54
Nitrogen (blue, ring)	0.056 375
Nitrogen (blue, NO <sub>2</sub> )	0.860 625
Oxygen (red)	-0.4585
Hydrogen (silver)	0.27
Atom group	Dipole moment magnitude ( $D$ )
CH <sub>2</sub> (centered at C)	1.652
NO <sub>2</sub> (centered at N)	-2.671
N-NO <sub>2</sub> (centered at NO <sub>2</sub> N)	-2.306

atoms. The ring flexibility is important (especially its dihedral and angular DOFs) as judged by the poor performance of models IV and V in predicting elastic moduli and thermal expansion, and since these interactions do not take much computational time, they should not be removed. The pair-wise force interactions comprise Coulomb interactions and short-range van der Waals interactions. The short ranged van der Waals interactions must be represented explicitly among nearest neighboring molecules to ensure that molecules do not overlap. The other computationally expensive interactions are the Coulomb interactions; these are proportional to  $Q^2$ , where  $Q$  is the number of charge centers. Since the RDX molecule is electrically neutral, intermolecular Coulombic interactions can be reasonably approximated by dipoles and higher moments.

Table 2 shows the atomic charges [53] on the RDX molecule. If we use a first order charge approximation for the atomic groups, the CH<sub>2</sub> units become electrically neutral, but they have a net moment. Similarly, the NO<sub>2</sub> groups are approximately neutral (net charge of  $-0.0056e$ ) but preserve a moment. So if the three CH<sub>2</sub> and three NO<sub>2</sub> groups are replaced with six dipoles, the new number of pairwise Coulombic force computations within the molecule is reduced by a factor of  ${}^{21}C_2/{}^6C_2 = 14$ . The number of DOFs will still have to be 6 for each dipole to account for displacements and rotations. This can also allow a higher time-step as the C-H vibrations are no longer considered (see section C).

Let us summarize the above discussion. In sections 3.1 and 3.2 we studied the molecular DOFs that must be allowed in order to accurately capture the elastic-plastic behavior. In the previous paragraph, we looked at the problem in terms of computation time, and concluded that allowing for molecular flexibility does not impose a huge cost. However, the non-bonded pair-wise interactions and long-range solvers cost about 90% of the computation time, and we proposed several ways to reduce that cost. Instead of allowing for 21 charge centers, six dipoles can be considered. Whether these dipoles are rigid or flexible or simply mapped from the full atomic representation is a detail, but the number of pairwise Coulombic force computations can be reduced this way by about 14. The pair-wise van der Waals interactions can be cut-off beyond the nearest neighbor molecules leading to linear scaling. The long-range  $K$ -space solver which scales as  $M\log(N)$  can be reduced  $21*\log(21)/(12*\log(12)) = 2.1$  times, with the 12 charge centers around the six dipoles. There may be alternate and better dipole representations that represent the charge multipole expansion of the molecule to a greater accuracy, but this requires further investigation.



## 4. Conclusion

In this work we evaluate the effect of gradually rendering the RDX molecule rigid on various material parameters. This provides insight into the role of molecular flexibility in the mechanics of the crystal and provides guidance for the development of CG representations of such crystals. We focus on the elastic constants, lattice parameters, thermal expansion coefficients, the PN stress and the stacking fault energy. The fully refined and fully flexible atomistic model of the molecule, Model I, is taken as reference. It is concluded that Models II and III provide reasonably accurate predictions of the elastic constants, lattice parameters and their dependence on pressure, and of the thermal expansion coefficients. This indicates that these properties do not depend in an essential way on the axial deformation of the bonds of the ring and N–N bonds. CG models of this type are acceptable as long as crystals with no defects are considered. The model in which the flexibility of the molecule is entirely removed, Model V, leads to large errors even for perfect crystals. The evaluation of the PN stress of dislocations and the stacking fault energy with all models considered leads to large errors. It results that all components of molecular flexibility are important when the lattice is subjected to large distortions as in the core of dislocations. The effect is more pronounced as the dislocation moves across Peierls barriers and the core distorts. The analysis indicates that no CG model that restricts molecular flexibility can capture accurately the motion of dislocations, which is the physical basis of plasticity.

It should be noted in relation to coarse graining that the present analysis is performed without modifying the force field, which is a necessary step when developing reduced models. Therefore, the errors discussed are due entirely to limiting the flexibility of the molecule and are necessarily present in any model in which effective interactions between CG groups of atoms are implemented. The data indicates in which conditions and for which crystal-scale parameters it is worth developing CG potentials and hence a full CG model.

## Acknowledgments

Support from the Army Research Office through grant W911NF-09-1-0330 is gratefully acknowledged. All simulations were performed at the Centre for Computational Innovations (CCI) and the Scientific Computations Research Center (SCOREC) at Rensselaer Polytechnic Institute.

## References

- [1] Thakkar A L, Hirsch C A and Page J G 1977 Solid dispersion approach for overcoming bioavailability problems due to polymorphism of nabilone, a cannabinoid derivative *J. Pharm. Pharmacol.* **29** 783–4
- [2] Lin S-Y, Hsu C-H and Ke W-T 2010 Solid-state transformation of different gabapentin polymorphs upon milling and co-milling *Int. J. Pharm.* **396** 83–90
- [3] Mathew N and Picu R C 2011 Molecular conformational stability in cyclotrimethylene trinitramine crystals *J. Chem. Phys.* **135** 024510
- [4] Cawkwell M J, Ramos K J, Hooks D E and Sewell T D 2010 Homogeneous dislocation nucleation in cyclotrimethylene trinitramine under shock loading *J. Appl. Phys.* **107** 063512
- [5] Pal A and Picu R C 2014 Rotational defects in cyclotrimethylene trinitramine (RDX) crystals *J. Chem. Phys.* **140** 044512
- [6] Boyd S, Murray J S and Politzer P 2009 Molecular dynamics characterization of void defects in crystalline (1,3,5-trinitro-1,3,5-triazacyclohexane) *J. Chem. Phys.* **131** 204903



- [7] Müller-Plathe F 2002 Coarse-graining in polymer simulation: from the atomistic to the mesoscopic scale and back *Chem. Phys. Chem.* **3** 754–69
- [8] Riniker S, Allison J R and Gunsteren W F van 2012 On developing coarse-grained models for biomolecular simulation: a review *Phys. Chem. Chem. Phys.* **14** 12423–30
- [9] Kraczek B and Chung P W 2013 Investigation of direct and indirect phonon-mediated bond excitation in  $\alpha$ -RDX *J. Chem. Phys.* **138** 074505
- [10] Gee R H, Wu C and Maiti A 2006 Coarse-grained model for a molecular crystal *Appl. Phys. Lett.* **89** 021919
- [11] Kroonblawd M P, Sewell T D and Maillet J-B 2016 Characteristics of energy exchange between inter- and intramolecular degrees of freedom in crystalline 1,3,5-triamino-2,4,6-trinitrobenzene (TATB) with implications for coarse-grained simulations of shock waves in polyatomic molecular crystals *J. Chem. Phys.* **144** 064501
- [12] Izvekov S, Chung P W and Rice B M 2010 The multiscale coarse-graining method: assessing its accuracy and introducing density dependent coarse-grain potentials *J. Chem. Phys.* **133** 064109
- [13] Izvekov S, Chung P W and Rice B M 2011 Particle-based multiscale coarse graining with density-dependent potentials: application to molecular crystals (hexahydro-1,3,5-trinitro-s-triazine) *J. Chem. Phys.* **135** 044112
- [14] Moore J D, Barnes B C, Izvekov S, Lísal M, Sellers M S, Taylor D E and Brennan J K 2016 A coarse-grain force field for RDX: density dependent and energy conserving *J. Chem. Phys.* **144** 104501
- [15] Noid W G, Chu J-W, Ayton G S, Krishna V, Izvekov S, Voth G A, Das A and Andersen H C 2008 The multiscale coarse-graining method: I. A rigorous bridge between atomistic and coarse-grained models *J. Chem. Phys.* **128** 244114
- [16] Noid W G, Liu P, Wang Y, Chu J-W, Ayton G S, Izvekov S, Andersen H C and Voth G A 2008 The multiscale coarse-graining method: II. Numerical implementation for coarse-grained molecular models *J. Chem. Phys.* **128** 244115
- [17] Munday L B, Chung P W, Rice B M and Solares S D 2011 Simulations of high-pressure phases in RDX *J. Phys. Chem. B* **115** 4378–86
- [18] Weingarten N S and Sausa R C 2015 Nanomechanics of RDX single crystals by force-displacement measurements and molecular dynamics simulations *J. Phys. Chem. A* **119** 9338–51
- [19] Smith G D and Bharadwaj R K 1999 Quantum chemistry based force field for simulations of HMX *J. Phys. Chem. B* **103** 3570–5
- [20] Sewell T D and Bennett C M 2000 Monte Carlo calculations of the elastic moduli and pressure-volume-temperature equation of state for hexahydro-1,3,5-trinitro-1,3,5-triazine *J. Appl. Phys.* **88** 88–95
- [21] Zheng L and Thompson D L 2006 Molecular dynamics simulations of melting of perfect crystalline hexahydro-1,3,5-trinitro-1,3,5-s-triazine *J. Chem. Phys.* **125** 084505
- [22] Pereverzev A, Sewell T D and Thompson D L 2013 Molecular dynamics study of the pressure-dependent terahertz infrared absorption spectrum of  $\alpha$ - and  $\gamma$ -RDX *J. Chem. Phys.* **139** 044108
- [23] Bedrov D, Hooper J B, Smith G D and Sewell T D 2009 Shock-induced transformations in crystalline RDX: a uniaxial constant-stress Hugoniotat molecular dynamics simulation study *J. Chem. Phys.* **131** 034712
- [24] Mathew N, Picu C R and Chung P W 2013 Peierls stress of dislocations in molecular crystal cyclotrimethylene trinitramine *J. Phys. Chem. A* **117** 5326–34
- [25] Mathew N and Picu R C 2013 Slip asymmetry in the molecular crystal cyclotrimethylenetrinitramine *Chem. Phys. Lett.* **582** 78–81
- [26] Munday L B, Mitchell R L, Knap J and Chung P W 2013 Role of molecule flexibility on the nucleation of dislocations in molecular crystals *Appl. Phys. Lett.* **103** 151911
- [27] Ramos K J, Hooks D E, Sewell T D and Cawkwell M J 2010 Anomalous hardening under shock compression in (021)-oriented cyclotrimethylene trinitramine single crystals *J. Appl. Phys.* **108** 066105
- [28] Choi C S and Prince E 1972 The crystal structure of cyclotrimethylenetrinitramine *Acta Crystallogr. B* **28** 2857–62
- [29] Shinoda W, Shiga M and Mikami M 2004 Rapid estimation of elastic constants by molecular dynamics simulation under constant stress *Phys. Rev. B* **69** 134103
- [30] Kamberaj H, Low R J and Neal M P 2005 Time reversible and symplectic integrators for molecular dynamics simulations of rigid molecules *J. Chem. Phys.* **122** 224114

- [31] Ryckaert J-P, Ciccotti G and Berendsen H J C 1977 Numerical integration of the cartesian equations of motion of a system with constraints: molecular dynamics of *n*-alkanes *J. Comput. Phys.* **23** 327–41
- [32] Van Swygenhoven H and Weertman J R 2006 Deformation in nanocrystalline metals *Mater. Today* **9** 24–31
- [33] Kohanoff J 1994 Phonon spectra from short non-thermally equilibrated molecular dynamics simulations *Comput. Mater. Sci.* **2** 221–32
- [34] Plimpton S 1995 Fast parallel algorithms for short-range molecular dynamics *J. Comput. Phys.* **117** 1–19
- [35] Bolme C A and Ramos K J 2014 The elastic tensor of single crystal RDX determined by Brillouin spectroscopy *J. Appl. Phys.* **116** 183503
- [36] Cady H H 1972 Coefficient of thermal expansion of pentaerythritol tetranitrate and hexahydro-1,3,5-trinitro-s-triazine (RDX) *J. Chem. Eng. Data* **17** 369–71
- [37] Haussühl S 2009 Elastic and thermoelastic properties of selected organic crystals: acenaphthene, trans-azobenzene, benzophenone, tolane, trans-stilbene, dibenzyl, diphenyl sulfone, 2,2'-biphenol, urea, melamine, hexogen, succinimide, pentaerythritol, urotropine, malonic acid, dimethyl malonic acid, maleic acid, hippuric acid, aluminium acetylacetonate, iron acetylacetonate, and tetraphenyl silicon *Z. Für Krist.—Cryst. Mater.* **216** 339–53
- [38] Schwarz R B, Hooks D E, Dick J J, Archuleta J I and Martinez A R 2005 Resonant ultrasound spectroscopy measurement of the elastic constants of cyclotrimethylene trinitramine *J. Appl. Phys.* **98** 056106
- [39] Sun J, Shu X, Liu Y, Zhang H, Liu X, Jiang Y, Kang B, Xue C and Song G 2011 Investigation on the thermal expansion and theoretical density of 1,3,5-trinitro-1,3,5-triazacyclohexane *Propellants Explos. Pyrotech.* **36** 341–6
- [40] Sun B, Winey J M, Hemmi N, Dreger Z A, Zimmerman K A, Gupta Y M, Torchinsky D H and Nelson K A 2008 Second-order elastic constants of pentaerythritol tetranitrate and cyclotrimethylene trinitramine using impulsive stimulated thermal scattering *J. Appl. Phys.* **104** 073517
- [41] Taylor D E 2014 Pressure dependent elastic constants of alpha and gamma cyclotrimethylene trinitramine: a quantum mechanical study *J. Appl. Phys.* **116** 053513
- [42] Hooks D E, Ramos K J, Bolme C A and Cawkwell M J 2015 Elasticity of crystalline molecular explosives *Propellants Explos. Pyrotech.* **40** 333–50
- [43] Davidson A J, Oswald I D H, Francis D J, Lennie A R, Marshall W G, Millar D I A, Pulham C R, Warren J E and Cumming A S 2008 Explosives under pressure—the crystal structure of  $\gamma$ -RDX as determined by high-pressure x-ray and neutron diffraction *Cryst. Eng. Commun.* **10** 162–5
- [44] Haycraft J J, Stevens L L and Eckhardt C J 2006 The elastic constants and related properties of the energetic material cyclotrimethylene trinitramine (RDX) determined by Brillouin scattering *J. Chem. Phys.* **124** 024712
- [45] Barron T H K 1998 Generalised theory of thermal expansion of solids *Thermal Expansion of Solids* ed C Y Ho vol 1–4 (New York: ASM) pp 1–108
- [46] Grüneisen E 1912 Theorie des festen zustandes einatomiger elemente *Ann. Phys.* **344** 257–306
- [47] Das D, Jacobs T and Barbour L J 2010 Exceptionally large positive and negative anisotropic thermal expansion of an organic crystalline material *Nat. Mater.* **9** 36–9
- [48] Connick W and May F G J 1969 Dislocation etching of cyclotrimethylene trinitramine crystals *J. Cryst. Growth* **5** 65–9
- [49] Halfpenny P J, Roberts K J and Sherwood J N 1984 Dislocations in energetic materials *J. Mater. Sci.* **19** 1629–37
- [50] Ramos K J, Hooks D E and Bahr D F 2009 Direct observation of plasticity and quantitative hardness measurements in single crystal cyclotrimethylene trinitramine by nanoindentation *Phil. Mag.* **89** 2381–402
- [51] McDermott I T and Phakey P P 1971 A method of correlating dislocations and etch pits: application to cyclotrimethylene trinitramine *J. Appl. Crystallogr.* **4** 479–81
- [52] Izvekov S, Chung P W and Rice B M 2011 Non-equilibrium molecular dynamics simulation study of heat transport in hexahydro-1,3,5-trinitro-s-triazine (RDX) *Int. J. Heat Mass Transf.* **54** 5623–32
- [53] Bedrov D, Ayyagari C, Smith G D, Sewell T D, Menikoff R and Zaug J M 2001 Molecular dynamics simulations of HMX crystal polymorphs using a flexible molecule force field *J. Comput.—Aided Mater. Des.* **8** 77–85